JOURNAL OF PROPULSION AND POWER
Vol. 23, No. 6, November–December 2007

Flow Choking by Drag and Combustion in Supersonic Engine Testing

Tohru Mitani* and Kouichiro Tani†
Japan Aerospace Exploration Agency, Miyagi 981-1525, Japan
and
Hiroshi Miyajima‡
Japan Aerospace Exploration Agency, Sagamihara 229-8510, Japan

DOI: 10.2514/1.30264

Breakdown of diffuser flow in the engine wind tunnel has often been observed during scramjet engine tests conducted in the Ramjet Engine Test Facility in Japan. The unstable and precipitant nature of the breakdown phenomena may result in serious damage to the engine wind tunnel and should therefore be prevented. A one-dimensional analysis was applied to the diffuser flow to identify the causes of the flow breakdown. All the losses and gains by the engine were represented by point sources of mass, momentum, and energy. The duct friction term was integrated along the diffuser, assuming that the normal shock was located at the exit of the duct. The thermal choking condition was calculated by incorporating results of a chemical equilibrium numerical code. The fuel rates causing the flow choking were successfully reproduced and matched with the limit of fuel rates observed in our tests. Inlet unstart of the engine caused the loss of the ejector-pumping effect in the diffuser system, which triggered flow choking. Choking was also promoted by the drag of the gas sampling rakes. The choking in diffuser flow and the engine unstart may be coupled, resulting in hysteresis in the diffuser breakdown, which was also experienced in our tests. As the rocket-based, combined-cycle engine is scheduled to be tested under the Mach 4 condition in 2007, the safety of the experiment is now a primary issue. The current analysis showed that the new engine would easily cause choking of diffuser because of the larger propellant supply rates and the relatively low specific impulse. Reasonable operation of the wind tunnel to control the flow choking in future tests was examined.

Nomenclature

C_d	=	total drag coefficients around engine
c_p	=	specific heat, 1.1 kJ/kg · K
c_{wf}	=	wall friction coefficient
D_{eg}	=	Drag of engine
d_h	=	diameter of diffuser, 0.78 m
I_{spf}	=	fuel-based specific impulse, km/s, defined as $\Delta F/m'$, $=u'$
L	=	length of diffuser ↖ 9.02 m ↗
M	=	Mach number of diffuser flow
m	=	mass flow rate of air, kg/s
m'	=	mass flow rate of propellant supplied to test engine (fuel for scramjet case; fuel and oxidizer for rocket-based, combined-cycle case)
P_{CJ}	=	Chapman–Jouguet detonation pressure
P_{suc}	=	backpressure in diffuser, =suction pressure of air evacuation system
P_V	=	test cell pressure
P^0	=	total pressure of the airflow
Q_c	=	heat of combustion of H_2, 121 MJ/kg
Q_w	=	latent heat of vaporization of water ↖ 9.02 MJ/kg ↗
T^0	=	total temperature of air (872 K in Mach 4, 1500 K in Mach 6 and 2500 K in Mach 8 flight conditions)
u	=	flow velocity of the air, km/s
u'	=	specific impulse based on the thrust increment by the fuel injection and combustion, km/s
W	=	molecular weight of air in diffuser
x	=	streamwise distance along diffuser
ΔF	=	thrust increment by fuel injection and combustion
$\Delta T'^0$	=	heat addition by engine combustion
γ	=	specific heat ratio
0	=	entrance of diffuser
1	=	engine
2	=	water spray vaporization point
3	=	shock wave and heat release by combustion
4	=	exit of diffuser

Subscripts

E	=	auxiliary ejector
w	=	water spray
$*$	=	choking point

Received 5 February 2007; revision received 14 May 2007; accepted for publication 2 June 2007.

*Fellow, Combined Propulsion Research Group. Member AIAA.
†Senior Researcher, Combined Propulsion Research Group. Member AIAA.
‡Collaborative Researcher.

I. Introduction

IN THE series of experiments conducted in the Ramjet Engine Test Facility in Japan, the hydrogen-fueled scramjet delivered net thrusts exceeding the engine drags and exhibited fuel specific impulses of about 10 km/s under Mach 4–8 flight conditions [1–4]. In some experiments, however, with increases of thrust in the scramjet engines, we often encountered "*engine unstart*" with subsequent, "*diffuser breakdown*" [5]. Engine unstart is defined as a phenomenon in which an excess supply of fuel to engines causes boundary-layer separation in the combustor and interference with the inlet flow by the separation bubble. In engine unstart, the engine expels a flame from the inlet and loses thrust drastically. In the case of the Mach 4 and 6 tests, engine unstart could be controlled by using boundary-layer bleeding and multistaged fuel injection. In the diffuser breakdown condition, the combustion gas blows back from the diffuser of the wind tunnel to the test cell. The blowback of the combustion gas and unburnt fuel increases the pressure and hydrogen concentration in the test cell, endangering the wind-tunnel

system. Therefore, we have to identify the mechanism of the diffuser breakdown to control it.

A rocket-based, combined-cycle (RBCC) engine [6] is now under research to deliver thrust to accelerate the vehicle from Mach 0 to the space speed of Mach 25. The engine works in the ejector-jet mode in the takeoff stage to Mach 3 and is then switched to the ramjet mode. Around Mach 7, the scramjet mode takes over. The rockets used in the ejector-jet mode will be used again in space where no air exists. Stationary engine tests for the ejector-mode are planned in the autumn of 2006 and Mach 4 engine testing in the ramjet mode is scheduled for the spring of 2007. There is a high possibility that the diffuser breakdown will occur in the RBCC engine (called "E3 engine") tests in our wind tunnel because a large amount of propellant will be supplied to drive the rockets installed inside the E3 engine [7].

In this study, the diffuser breakdown phenomenon observed in our wind tunnel was first examined in detail. A one-dimensional analysis was then applied to the diffuser flow to predict the effect of the engine and other components of the wind tunnel on the flow. In the analysis, the engine was simplified as a point source of mass, momentum, and energy. The wall frictional loss of the diffuser was evaluated by integrating the loss along the diffuser, assuming that normal shock was located at the exit of the constant diameter diffuser. With these simplified models, the fuel rates causing choking were successfully reproduced and matched with the limit fuel rates observed in our scramjet engine tests. We extended the analysis to cases of E3 engine tests and found that diffuser breakdown would easily occur in the engine tests. Based on the results, safer operation of the wind tunnel to control flow choking was examined.

II. Diffuser Breakdown

Figure 1 illustrates the ramjet engine test facility (RJTF), our engine wind tunnel used to test scramjet engines. The size of the cylindrical test cell is 3 m in diameter and 5 m in length. A facility nozzle, which has a rectangular exit cross section of 51 cm^2, is depicted at the left end in the figure. Heated air which simulates three distinctive flight conditions is supplied through the nozzle. Flow properties of T^0 and P^0 are 870 K/0.86 MPa, 1500 K/5 MPa, and 2500 K/10 MPa for Mach 4, 6, and 8 conditions, respectively. The engine is installed on a thrust bed and engine drag and thrust by combustion can be measured. Airflow and the engine exhaust are captured by a catch-cone and the static pressure is raised to match P_{suc} through a straight-duct diffuser with a diameter of 0.78 m and a length of 9.02 m. A two-staged steam ejector system is connected to the diffuser to maintain P_{suc} at 29 kPa at Mach 4 to 6.9 kPa at Mach 8 conditions. In the actual facility, upstream of the catch-cone, there is a jet stretcher which has a pair of diagonal openings one-sixth of the circumference. For the sake of clarity, the stretcher is deleted in Fig. 1. Wall pressures of the engine as well as some facility pressure data (e.g., diffuser wall pressure) were measured by the electric scanning device at 200 Hz sampling rate. Its end-to-end uncertainty was 0.5% of its full scale. The thrust bed, which is depicted as FMS (force measurement system), can measure the thrust or drag up to 7000 N. The error of FMS was estimated by the repeated tests with the same condition, and was found to be ±50 N.

Figure 2a depicts the engine-unstart condition when an excess amount of fuel was supplied to the engine. The picture shows combustion gas issuing out upstream of the cowl edge. Although spilled flow raised the test cell pressure substantially, the flow seemed to be exhausted. As will be discussed later, in this particular case, the ejector was in a backpressure dependent operation mode, i.e., diffuser breakdown was encountered as soon as fuel was supplied to the engine. It should be noted that there were cases in which engine unstart did not immediately lead to diffuser breakdown.

Figure 2b shows the pulsative combustion of the hydrogen fuel accumulated in the test cell, which was observed in the engine test, catalogued as Mach 8–12. The large pressure increase caused the nozzle flow to separate from the bottom surface of the facility nozzle. Unburned hydrogen reversed from the engine to the facility nozzle and a flame issued from the inside of the facility nozzle. Intermittent

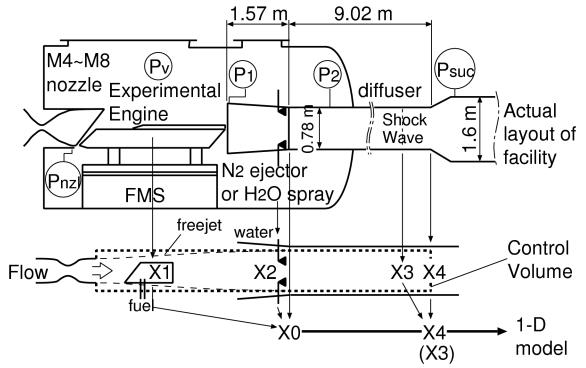

Fig. 1 Ramjet engine test facility for scramjet and RBCC engines and its analysis model.

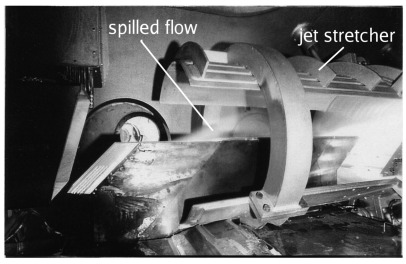

a) Engine unstart

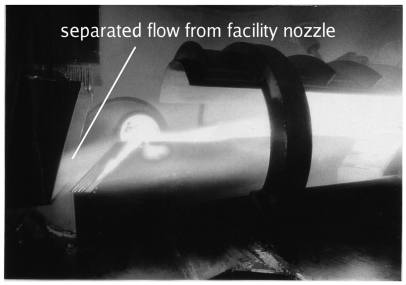

b) Pulsative comb

Fig. 2 Diffuser break in Mach 8–12 engine test.

combustion reoccurred three times as will be shown later. The test cell pressure increased from 1.5 to 10 kPa and damaged some of the pressure sensors. This phenomenon was accompanied by a large noise and high H_2 concentration in the test cell, exceeding our safety limit of 5000 ppm during the engine test. The diffuser breakdown is clearly a dangerous phenomenon to be avoided in wind-tunnel experiments. If it is somehow inevitable in engine tests, a reasonable operation procedure has to be employed.

III. Thermal Choking in Diffusers

One condition for maintaining supersonic-flow wind tunnels is that the total pressure in the diffuser is sufficiently high to exhaust the flow against the backpressure at the diffuser exit. The other condition is that the flow can run through the diffuser without choking. These are the necessary and sufficient conditions for starting operation of supersonic engine wind tunnels. The second condition is especially significant for engine wind tunnels because relatively large test articles are tested and large heat release is inevitable.

For instance, in our tests, the Mach number at the diffuser entrance is evaluated to be from 4.14 in the Mach 4 flight condition to 7.85 in the Mach 8 condition. The limit of fuel (H_2) supply rate causing thermal choking in the diffuser is simply given by a function of M_0 [8].

$$1 + \frac{Q_c}{c_p T^0} \cdot \frac{m'^*}{m} = \frac{(1+\gamma \cdot M_0^2)^2}{2(1+\gamma) \cdot M_0^2[1+(\gamma-1)/2M_0^2]} \qquad (1)$$

$$\frac{dy}{y} = \frac{-1}{y-1} \times \left[\begin{array}{ll} (1+ay)\cdot \left\{ \begin{array}{l} 2\cdot(1+\gamma\cdot y)\cdot \frac{m'}{m}\delta(x-x1)dx\text{: mass} \\ +\gamma\cdot C_d y\delta(x-x1)dx\text{: drag} \\ -2\gamma\cdot\left(\frac{u'}{u}\frac{m'}{m}\right)\cdot y\delta(x-x1)dx\text{: thrust} \end{array} \right\} & \text{: engine}(x_1) \\ +(1+\gamma\cdot y)\cdot \left\{ \begin{array}{l} (1+ay)\cdot\left(2\frac{m_w}{m}+\frac{\Delta T_w^0}{T^0}\right) \\ -\frac{\Delta W_w}{W} \end{array} \right\}\delta(x-x2)dx & \text{: spray}(x_2) \\ +4\gamma\cdot c_{\mathrm{wf}}\cdot y(1+ay)\frac{dx}{d_h} & \text{: wall drag in diffuser} \end{array} \right] \tag{4}$$

When the specific heat ratio is assumed to be 1.4 and constant c_p and Q_c are postulated, allowable H_2 supply rates are calculated to be from 0.262 kg/s (Mach 4) to 0.161 kg/s (Mach 8), both of which fall near the typical fuel rate of the experiments. Thus the test conditions in our engine tests are close to the thermal choking limit. Therefore, the accurate allowable H_2 supply rates and maximum pressure in the test cell in the choking condition must be evaluated in advance of the engine tests.

In the experiments, the test engine is installed on the thrust bed and the engine and the support rig exert drag on the airflow. The engine thrust works as an ejector to the airflow when the engine delivers a thrust by combustion. The amount of heat release may depend on the chemical equilibrium because of the high combustion temperature and low pressure in the diffuser flow. Therefore, precise estimation of the Mach number and total pressure in diffuser flow are required to access the maximum fuel supply rate that causes thermal choking.

IV. Equation for Diffuser Choking

A. Effects of Engine on Airflow

The freejet from the square facility nozzle has a complicated three-dimensional flow around the engine and finally attaches to the duct near the inlet of the straight diffuser duct, still maintaining supersonic speed. As was depicted in Fig. 1, in this analysis, the control volume was defined as a simple cylinder which has one end at the facility nozzle and the other at the diffuser exit with the diameter of the diffuser duct. Downstream of the point of the attachment on the diffuser lip, the flow is assumed to be one-dimensional. One of the momentum errors which are generated at the entrance of the diffuser duct is the product of the P_V and the area difference between the duct and facility nozzle, which turned out to be small. Another error might appear when the flow attaches to the duct in the conical portion. The extra pressure drag, which is the axial component of the product of conical area and pressure on the cone, and also the friction drag on the cone wall may be taken into consideration. However, in this analysis, the flow is assumed to attach to the straight duct lip and the drag on the cone is neglected.

With previously mentioned assumptions and by defining y and a as

$$y \equiv M^2 \tag{2}$$

$$a \equiv \frac{\gamma-1}{2} \tag{3}$$

one can express the Mach number in the diffuser in the following one-dimensional form:

where the engine to be tested, as shown in Fig. 1, is installed at x_1 and water spray to cool the air temperature is at x_2. ΔT_w^0, which appears in the term of spray effect, is defined as

$$\Delta T_w^0 = \frac{-Q_w}{C_p}\cdot\frac{m_w}{m} \tag{5}$$

It should also be noted that the effect at each location was condensed at a single point by introducing Dirac's delta function δ. The wall of the diffuser has a friction coefficient of c_{wf}, which will be evaluated in a later section. The diameter of the straight duct is denoted by d_h.

The engine at x_1 plays four roles: mass addition, drag, thrust, and heat addition. The effect of mass addition is governed by the ratio of m'/m. The m is the mass flow rate of incoming air, varying from 46.3 kg/s (Mach 4) to 7.9 kg/s (Mach 8). The H_2 supply rate to the engine is denoted by m' and typical rates are 0.2 kg/s (Mach 4) and 0.1 kg/s (Mach 8). Therefore, the mass flow ratio m'/m was a small parameter from 0.005 to 0.01 in the scramjet engine tests. However, the m'/m may become as large as 0.3 in the E3 engine tests in the Mach 8 condition.

The drag coefficient in Eq. (4), i.e., C_d, is defined as the normalized value of all the drag forces by the dynamic pressure and cross-sectional area of the duct. Here, the drag forces include the engine drag, drag caused by the support rigs and drag due to gas sampling rakes if they are inserted downstream of the engine nozzle.

The engine thrust produces an ejector effect if $u'/u \gg 1$ in Eq. (4). The overall role of fuel combustion is examined by combination of the mass and momentum additions.

$$\left(1-\frac{u'}{u}\right)\frac{m'}{m} \tag{6}$$

The unity in the bracket corresponds to the mass addition. The exhaust velocity of the engine u' can be expressed by the fuel-based specific impulse, i.e., $u' = I_{\mathrm{spf}} = \Delta F/m'$. It should be noted that the fuel specific impulse defined here is not the commonly used one that is defined as thrust-minus-drag divided by fuel flow rate. Instead, in this analysis, ΔF, which is a thrust increment due to fuel injection and combustion, is divided by the fuel flow rate m'. ΔF is tabulated as ΔF_{exp} and can be found in Table 1 in [3]. The fuel flow rate m' can also be obtained from the stoichiometric H_2 rate given as m_{H2} and Φ, in the same table of the reference. The typical I_{spf} was found to be from 9.5 km/s (Mach 8 condition) to 23.3 km/s (Mach 6 condition) in our scramjet engine tests with the boundary-layer ingestion. Because the air velocity u varied from 1.165 km/s (Mach 4) to 2.547 km/s (Mach 8), the magnitude of the bracket in front of m'/m is on the order of 10. This means that the engine works as an ejector pump to accelerate the airflow, if and only if the engine delivers a thrust.

As will be described in Sec. IV.C, Chemical Equilibrium Calculation, the flow properties at the exit of the diffuser can be

obtained by assuming that all the chemical reactions occur at the location x_4, and the heat release in the engine at x_1 is reflected in the thrust term.

The effects of the water spray, if installed at x_2, are the mass addition of water and reductions of air temperature and molecular weight in the air–water mixture. Considering the rather smaller size of the engine in comparison with the 9.02-m-long diffuser, the engine can be treated as a point source of mass, momentum, and energy located at x_1. The water spray can also be approximated to be a point source of mass and a point sink of energy at x_2. Conservations of mass, momentum, and energy between the entrance and exit of the diffuser are of importance in the current analysis, the point sources at x_1 and x_2 were then degenerated into a single point source at x_0. By integrating the wall drag term in Eq. (4), flow properties just upstream of x_3 can be obtained. A chemical equilibrium calculation [9] was carried out to satisfy the mass, momentum, and energy across the combustion and shock wave located at x_3 and, finally, all flow properties at x_4 could be obtained.

First, the effects at x_1 were considered by solving the terms related to x_1. Again, here, two constants are introduced as

$$b \equiv \frac{2m'}{m}$$

$$c \equiv \gamma \cdot \left\{ C_d + 2 \cdot \left[\left(1 - \frac{u'}{u} \right) \cdot \frac{m'}{m} \right] \right\} \tag{7}$$

to obtain the following differential equation which is the "engine" part of Eq. (4).

$$\frac{dy}{y} = \frac{-(1 + a \cdot y)(b + c \cdot y)}{y - 1} \cdot \delta(x) dx \tag{8}$$

By integration across the point source from x_- to x_+, the variation of Mach number was determined.

$$[\ell_n \{ y^{\frac{1}{b}} |1 + a \cdot y|^{\frac{a+1}{c-ab}} |b + c \cdot y|^{-\frac{1}{bc-ab}} \}]_{y_-}^{y_+} = 1 \tag{9}$$

The variation of total pressure across the point source was also derived after changing the independent variable from x to y, which is given by

$$\frac{P^0|_+}{P^0|_-} = [\{ |1 + a \cdot y|^{-\frac{a+1}{a(c-ab)}} |b + c \cdot y|^{\frac{b+c}{c(c-ab)}} \}^{-\frac{\epsilon}{2}}]_{y_-}^{y_+} \tag{10}$$

All the flow properties could be calculated from M_+ and P_+^0. When the water spray is applied, the T_+^0 can be calculated from the energy conservation.

The friction drag exerted all along the 9.02-m-long diffuser duct may be overestimated when c_{wf} is approximated solely based on the properties at the diffuser entrance. The Mach number dependence of c_{wf} is given as follows [10]:

$$c_{wf} = \frac{c_{wf0}}{[1 + (\gamma - 1)/2M^2]^\alpha} \tag{11}$$

where c_{wf0} denotes the wall friction coefficient at a limit of $M = 0$. For the power (α) which expresses the Mach number dependence, $\alpha = 0.467$ is recommended [10]. However, by rounding off α to 0.5, a closed form can be derived from Eq. (4):

$$\int_{y_{0+}}^{y_{3-}} \frac{(1 - y)\, dy}{y^2 \sqrt{1 + ay}} = 4\gamma c_{wf0} \frac{L}{d_h} \tag{12}$$

By integrating Eq. (12), one can obtain

$$\left[-\frac{\sqrt{1 + ay}}{y} + \left(1 + \frac{a}{2} \right) \ell_n \left(\frac{\sqrt{1 + ay} - 1}{\sqrt{1 + ay} + 1} \right) \right]_{y_{0+}}^{y_{3-}} = 4\gamma c_{wf0} \frac{L}{d_h} \tag{13}$$

where y_{3-} corresponds to the square of the Mach number just upstream of the shock wave which was assumed to exist near the end of the diffuser duct. In the same way, the static pressure at x_{3-} can be obtained in the following form:

$$\frac{P_{3-}}{P_{0+}} = \sqrt{\frac{y_{0+}(1 + ay_{0+})}{y_{3-}(1 + ay_{3-})}} \tag{14}$$

Because the current analysis is based on the one-dimensional model, the accuracy primarily depends on the radial uniformity of the flow inside the diffuser. The input values of facility and engines also directly affect the uncertainty. Most uncertain data are drag-of-engine support rigs and the gas sampling rakes, because they were hard to measure. From the comparison with the data of many experiments, we believe that the overall error of the limit fuel rate, for diffuser breakdown, is within 30%.

B. Choking in Engine Wind Tunnels

Figure 3 indicates the effect of engine drag on the total pressure behind the engine (x_1) in the Mach 4 condition. The slight reduction of P^0 from 0.86 MPa at $C_d = 0$ (i.e., a negligible drag) with $I_{spf} = 0$ in Fig. 3 is caused by the fuel addition of $m' = 0.2$ kg/s. Thus the mass addition is a small perturbation in the P^0 because of the magnitude of m'/m found in Eq. (4).

The P^0 decreased with increasing C_d of the engine, support rig and probe rakes. The P^0 was decreased from 0.86 to 0.22 MPa at $C_d = 0.2$ and 0.1 at $C_d = 0.5$. On the other hand, the engine specific impulse of $I_{spf} = 15$ km/s raised the P^0, cancelling the effect of drag of $C_d = 0.11$, to recover P^0 to 0.86 MPa.

Figure 3 also shows that the P^0 downstream of the engine asymptotically approached 0.1 MPa with increasing C_d irrespective of I_{spf}. The P^0 at x_4 was calculated assuming a shock wave between x_2 and x_4. The pressure loss across the shock wave was small because the Mach number was close to unity, as can be seen in Fig. 4, which will be shown later. As a result, the P^0 was sufficiently higher with a safety factor of three than the backpressure P_{suc}, as is illustrated by the horizontal line in Fig. 3. This result implies that the airflow can be exhausted against P_{suc} in the test condition up to $C_d = 0.5$.

Figure 4 illustrates effects of engine drag and the specific impulse on the Mach number downstream of the engine. The flow Mach number decreased from 2.5 ($C_d = 0.2$) to 1.5 ($C_d = 0.5$) when the engine thrust was negligible. When an engine produced thrust, i.e., a positive specific impulse, the ejector effect increased the Mach number in the diffuser.

However, even in the case with $I_{spf} = 15$ km/s, the Mach number decreased below two if the engine had a large drag of $C_d = 0.5$. Because of the denominator of $(y - 1)$ in Eq. (4), flow approaches to choking with increasing rate as y goes to one. This indicates that flow choking easily occurs in engine wind tunnels if large test articles (i.e., large C_d) with high heat release of combustion are tested. Typical static pressure in the engine wind tunnel is below atmospheric pressure and static temperature is above 2000 K. The gas flow in the

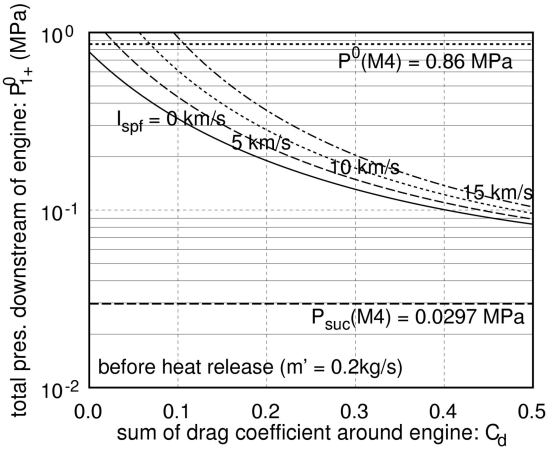

Fig. 3 Total pressure downstream of engine.

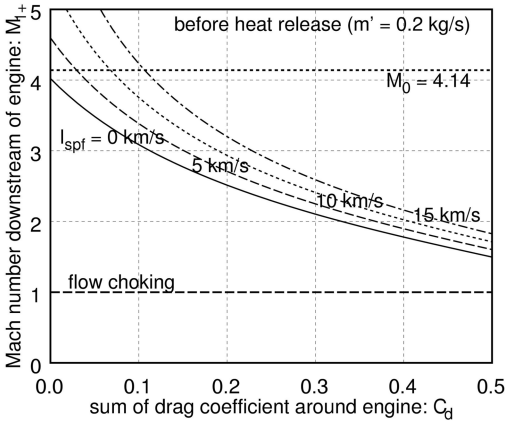

Fig. 4 Mach number downstream of engines.

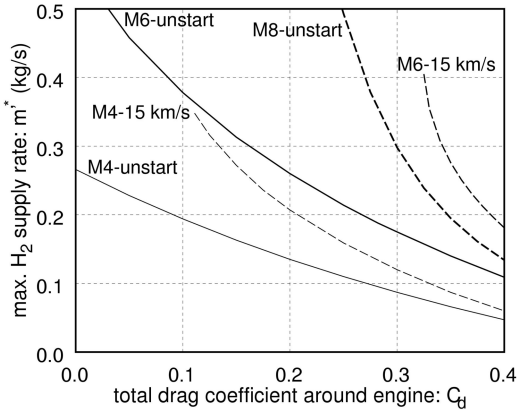

Fig. 5 Maximum H_2 supply rates causing thermal choking.

diffuser contains a great amount of H_2O. Therefore, chemical equilibrium calculations [9] are necessary for the shock wave and combustion.

C. Chemical Equilibrium Calculations

When the upstream condition is specified up to x_3 and the stream at the exit of the diffuser (x_4) is in a chemical equilibrium state, the location of heat release (schedule of combustion up to x_3, namely, combustion efficiency inside the scramjet engines at x_1) does not affect the final flow at x_4. The combustion efficiency in the engine is reflected in the thrust term (u'/u) in Eq. (4). Therefore, the flow properties downstream of the heat release and the shock wave at x_3 (i.e., x_{3+}) can be found by using a chemical equilibrium code with a specified Mach number, static pressure, static temperature, and concentration of H_2 at x_{3-} [9]. Figure 5 shows the maximum H_2 supply rate causing thermal choking as functions of C_d and I_{spf} for the Mach 4, 6, and 8 conditions. The lines labeled "-15 km/s" represent the limit of H_2 when the engine delivers thrust corresponding to $I_{spf} = 15$ km/s. The lines labeled "unstart" denote the cases when the engine is in unstart condition (i.e., $I_{spf} = 0$ km/s).

The line at the far right is a case of engine delivering specific impulse of $I_{spf} = 15$ km/s under the Mach 6 condition. This suggests that thermal choking does not occur in the Mach 6 and 8 tests unless the engine has a drag of C_d greater than 0.3. The reason for the greater margin is that the m'/m became larger and the ejector-pumping effect was dominant as derived from Eqs. (6) and (7). This tendency could also be confirmed by comparison of the shift of lines brought about by the specific thrust of $I_{spf} = 15$ km/s in the Mach 4 and 6 conditions. The limit H_2 line with the positive specific impulse for the Mach 6 condition moved farther right than that in the Mach 4 condition.

The stoichiometric H_2 rates in engine combustors were found to be 0.05 kg/s for the Mach 8 engine, 0.16 kg/s for the Mach 6 engine, and 0.2 kg/s for the Mach 4 engine. Therefore, the limit of the H_2 rate of the Mach 8 condition is a far richer condition compared with our engine test condition. However, the limit of H_2 rates from 0.32 to 0.16 kg/s in the M6 condition correspond to an equivalence ratio between two and one, and are close to our engine test region. The limit of H_2 rate in the Mach 4 condition was found to overlap our engine test range.

V. Scramjet Engine Tests

A. Four Engine Tests and Hysteresis

Figure 5 also indicates that the limit of the H_2 rate at $C_d = 0.2$ was 0.21 kg/s while the engine produces a positive specific impulse of $I_{spf} = 15$ km/s and it decreased to 0.14 kg/s when the engine lost the thrust (i.e., $I_{spf} = 0$) by falling into the unstart condition. This means that, at the moment of the engine unstart, the diffuser also chokes simultaneously. In another words, the engine unstart becomes a trigger for diffuser breakdown. In our engine tests, diffuser breakdown occurred at $m' = 0.2$ kg/s simultaneously with engine unstart.

Once the diffuser breakdown occurs, the pressure in the test cell rises and a wave emanating from the facility nozzle disturbs the inlet flow of the engine. Thus, the engine inlet flow cannot restart during the diffuser breakdown. This coupling of engine unstart and diffuser choking generates a hysteresis event resulting in engine–wind-tunnel interference.

There are two processes which induce engine unstart. The first one is due to the boundary-layer separation in combustor and inlet section in engines. Boundary-layer control, for instance bleeding in the inlet and/or isolator section, is effective to prevent such separation. Our engine test provided evidence that the maximum H_2 rate limited by the engine unstart could be increased threefold with a bleed of 3% of the incoming air. This bleed, however, is not practical for the second process of the engine unstart, namely, flow choking in the engine combustor.

As the flow choking in the combustor occurs by the same mechanism as discussed in the diffuser flow, the same analysis could be applied to the engine internal flow. The analysis yielded the maximum allowable fuel rate and the maximum thrust attained in a given engine geometry. These values have been used as the basis to quantify the engine performance relatively in actual engine tests [3]. The sonic combustion in the scramjet engine combustor, postulated to obtain the limit of the fuel flow rate, has been reproduced in computational fluid dynamics studies [11].

B. Gas Sampling in the Mach 6 and 8 Tests

In the Mach 6 engine test, C_d was found to be 0.172. Figure 5 implies that there is no possibility of diffuser choking as far as the engine delivers a maximum thrust corresponding to $I_{spf} = 15$ km/s. Based on this fact, we attempted to measure combustion efficiency by gas sampling in the condition in which the maximum thrust was achieved.

When we installed gas sampling rakes behind the engine nozzle, they produced an additional drag of $C_d = 0.11$ in the diffuser flow. The total drag of $C_d = 0.282$ yielded a choking limit around $m' = 0.19$ kg/s. This suggests that installing gas sampling rakes induces diffuser breakdown under the same condition in which a stable operation producing thrust of 3 kN at $m' = 0.2$ kg/s without the rakes attached. In an actual engine test with the gas sampling rakes, the diffuser breakdown was encountered. Presumably, engine unstart upon an increase of fuel flow rate was followed by diffuser breakdown. As a result, we failed to measure combustion efficiency at the best engine performance. When engines produce thrust, diffuser breakdown does not occur in the Mach 8 tests. However, the limit m' line appears in the region from $m' = 0.5$ to 0.1 kg/s when the engine does not start or falls into the unstart condition. The preliminary estimation of total drag coefficient C_d with the rakes in the Mach 8 condition was 0.32 and the limit of the fuel flow rate m' was around 0.2 kg/s, as shown by calculation. This value is substantially higher than that of the test (i.e., $m' = 0.11$ kg/s) shown

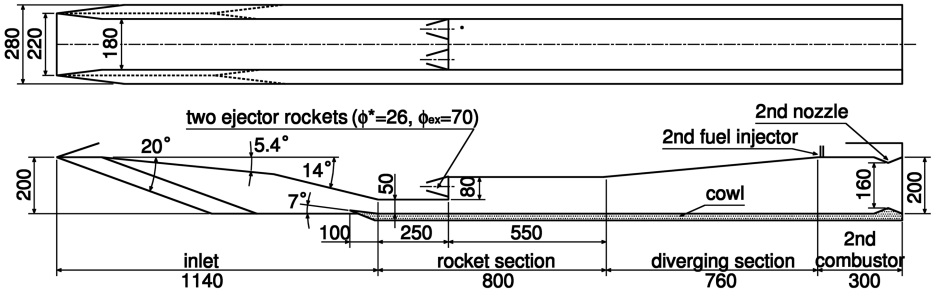

Fig. 6 E3 engine to be tested under the Mach 4 flight condition (propellant rate = 1.4–2.4 kg/s).

in Fig. 2. Considering the uncertainties in estimating precise drags in the Mach 8 condition, the agreement between the predicted and the observed limit of the fuel flow rates is reasonable. It can be concluded that current one-dimensional flow analysis consisting of the point source approximation and a chemical equilibrium code successfully duplicated the limit of the fuel rates causing thermal choking in our diffuser. The actual limit was observed with a slightly lower m'.

VI. E3 Engine in Mach 4 Flight Condition

A. E3 Engine and Evaluation of Thrust

Figure 6 presents configurations of our first rocket-based, combined-cycle (RBCC) engine (E3 engine). The entrance of the flow path is 220 mm wide and 200 mm high, and the compressed air is supplied to the combustor through the throat, which is 180 mm wide and 50 mm high. The engine contains two sets of rocket engines, each of which has a throat 26 mm in diameter and an exit 70 mm in diameter. The engine burns gaseous H_2 and O_2 with an O_2/H_2 mass ratio of seven [6]. The designed propellant rates are 1.4 kg/s at a combustion pressure of 3 MPa or 2.4 kg/s at 5 MPa. There are secondary fuel injectors in the secondary combustor downstream of the diverging section, and the secondary H_2 (max 0.06 kg/s) and remaining H_2 exhausted from the rockets burn with the air from the inlet. The combustion gas is accelerated to sonic speed at the exit throat, which is 160 mm in height and 180 mm in width, to be exhausted to the outer flow.

Component tests have been carried out using a subscale wind tunnel. The air capture ratio was found to be 0.4 and the pressure recovery performance was 0.7 in the inlet with the same type of configuration as E3 [12]. Based on these values, the combustion pressure in the secondary combustor was found to be 0.28 MPa and the I_{spf} to be 3.5 km/s.

Because thermal choking in the diffuser may be induced by engine unstart, we have to consider the engine performance under conditions of engine unstart. In the worst case scenario, when a separation bubble completely blocks the incoming flow, the rockets in the E3 engine produce a specific impulse of $I_{spf} = 1.4$ km/s. In a more realistic approximation of engine unstart, a normal shock wave is assumed ahead of the air throat and a part of the air is introduced into the combustor. In this case, the engine gives $I_{spf} = 2.8$ km/s with no secondary combustion.

B. Limit of the Fuel Rate in E3 Engine

The maximum allowable fuel rate was calculated assuming I_{spf} from 0 to 5 km/s with changing D_{eg} from 2 to 4 kN and is shown in Fig. 7. Note that, for the calculation, additional drags around the engine, such as engine support drag, had to be incorporated and its total value was fixed to be 2 kN in all cases. When the drag of the engine was greater than 4 kN, the maximum fuel rate decreased to a level less than 1.44 kg/s, which corresponds to the designed propellant rate of the rocket, even if the engine delivers a specific impulse of $I_{spf} = 3$ km/s. This suggests that the diffuser cannot swallow the air with the designed propellant rate when the engine falls into a lower performance condition. The limit of I_{spf} for safe operation decreases from 3 to 1.5 km/s as the engine drag decreases from 4 to 2 kN. However, engine drag of about 2 kN was predicted as a minimum value from the subscale wind-tunnel experiments [12]. This means that additional drag originating from the engine support and the windshield should be reduced as much as possible. When the engine falls into the unstart condition, the I_{spf} decreases to a level less than 2.5 km/s. Thus an engine test with D_{eg} greater than 3 kN may be dangerous under the unstart condition. Because the current gas sampling rakes cause an additional drag of 1.5 kN in the airflow, the gas sampling should be carried out with great caution.

C. Test Cell Pressure at Thermal Choking

Figure 8 illustrates pressure histories in the test cell, those measured on the diffuser wall, and at the nozzle exit in the Mach 8–12 test shown in Fig. 2. The test was conducted with the scramjet engine model, but the phenomenon that was observed in this experiment was suggestive for the safety operation of E3 engine test. Note that the locations of the sensors are indicated in Fig. 1. In this test, the wind tunnel was in a stable condition at 76 s and the fuel was supplied from 77.5 s. Because the engine fell into the unstart condition immediately after fuel was supplied, the test cell pressure jumped from 2.6 to 5.5 kPa. The separation of the boundary layer on the nozzle also raised the nozzle wall pressure from 1.5 to 3 kPa at 77.5 s. Pulsative combustion occurred from 82 s and spikes repeatedly appeared in the test cell and nozzle pressure histories three times. Because of the

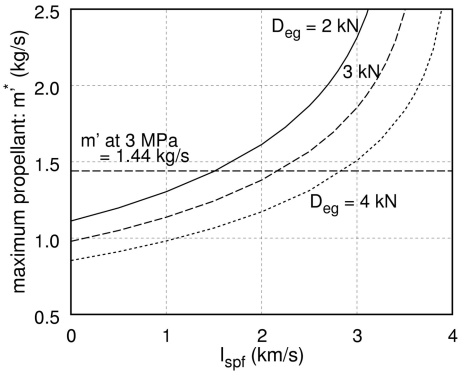

Fig. 7 Maximum fuel rate by thermal choking in the E3 tests.

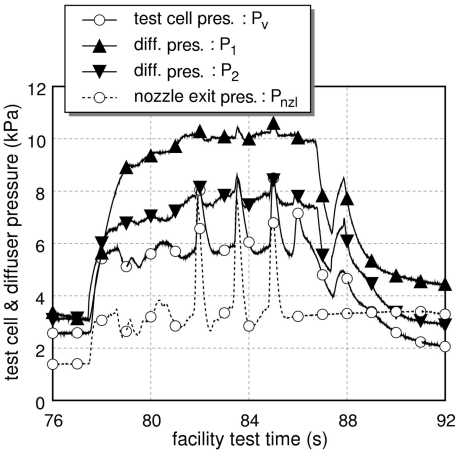

Fig. 8 Diffuser breakdown observed in a Mach 8 engine test.

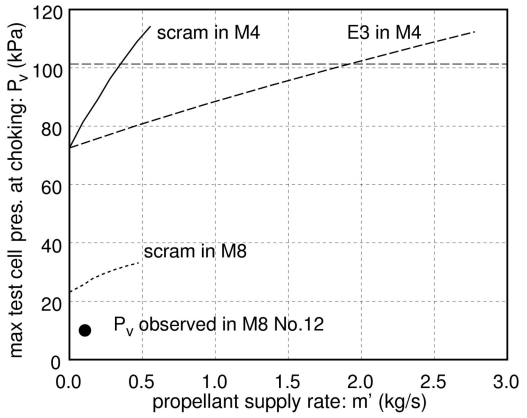

Fig. 9 Maximum cell pressure assuming combustion in test cell.

harsh pressure jump, the sensor at the nozzle exit wall was damaged at 85 s.

In Fig. 8, the sensor at the entrance of diffuser showed the highest pressure of 10 kPa and the sensor downstream of it indicated a lower pressure of 8 kPa. The pulsation in the test cell and the nozzle exit diminished in the diffuser. This suggests that combustion occurred in the test cell. From this observation, it is fair to assume that there was a small supersonic freejet containing a shock train and surrounded by a large subsonic stream. As a result, the flow downstream of the diffuser could be assumed to be subsonic. This allows the following evaluation of the maximum pressure in the test cell at the thermal choking in the diffuser.

Figure 9 presents the equilibrium pressure in the test cell in which the supplied air and fuel burn completely and the combustion gas is exhausted under the choke condition at the diffuser. First, the case of the Mach 8 test is examined. The combustion temperature increased from 2500 to 2970 K and the test cell pressure increased to 35 kPa with an increase in the H_2 rate to 0.5 kg/s. The circle indicates the pressure observed in the Mach 8–12 test. The comparison in Fig. 8 suggests that the approximation with the assumptions of complete combustion in the test cell and choking in diffuser tend to overestimate the test cell pressure by a factor of two.

The same approximation yielded the estimation for the E3 engine test in the Mach 4 condition in Fig. 9. When propellant was supplied to the E3 engine at 2.4 kg/s, the equilibrium cell pressure reached 110 kPa, exceeding atmospheric pressure. On the other hand, the test cell pressure could be lowered to 90 kPa when the propellant rate was restricted to 1.4 kg/s (the combustion pressure = 3 MPa).

A possible maximum pressure (the worst case) was considered assuming Chapman–Jouguet (C–J) detonation. The calculation for the C–J detonation reaction was conducted with the same numerical code as described earlier [9]. The C–J detonation in the Mach 4 and 8 conditions tended to overestimate the detonation pressure by a factor of four. Based on these experiences in our scramjet engine tests, E3 engine tests for the test cell pressure not exceeding 50 kPa can be conducted if the propellant rate is restricted to less than 1.4 kg/s.

D. Prevention of Thermal Choking

To avoid thermal choking in diffusers, we examined the effects of auxiliary ejectors driven by N_2 and water spray (at x_2) to cool the air. The effect of the N_2 ejector can be found by replacing m' and u' in Eq. (6) with those of the ejector properties m_E and u_E. The u_E is as large as 0.5 km/s when cold N_2 is used and much smaller than the $u = 1.16$ km/s of the air heated to $T^0 = 872$ K (the Mach 4). Therefore, the ejector driven by cold N_2 does not work nor lower the diffuser performance by mass addition.

A similar situation occurs in the case of use of water spray at the diffuser entrance. The effects of water spray on the Mach number change can be represented by the following equation in which contributions of mass, vaporization of water, and reduction of molecular weight are expressed as functions of the mass of water, m_W/m.

$$\frac{dy}{y} = \frac{-2(1+\gamma\cdot y)}{y-1}\cdot\left\{\left(1-\frac{Q_v}{2c_pT^0}+0.609\right) + a\left(1-\frac{Q_v}{2c_pT^0}\right)y\right\}\cdot\frac{m_w}{m} \tag{15}$$

The constant, 0.609, resulted from the change of molecular weight by water. The most dominant term on the right-hand side is that multiplied by the variable y.

$$\left(1-\frac{Q_w}{2\cdot c_pT^0}\right) \tag{16}$$

The effect of water spray is governed by competition between the mass addition and the cooling of water. The balanced temperature of the two effects was found to be 1500 K. Thus the two effects were cancelled out in the Mach 6 condition and the mass addition overcame the cooling effect, resulting in lowering of the diffuser performance in the Mach 8 condition. In the Mach 4 condition with $T^0 = 872$ K, the cooling effect was found to be negligible when the contribution of lowered molecular weight by water spray was included.

As far as the current analysis can be applied, there is no effective method to retard the thermal choking in diffusers in engine wind tunnels. In general, thermal choking can be avoided by reducing the size of the engine model or by increasing the diffuser cross-sectional area associated with increased pumping capacity if possible. However, when the size of engine is fixed and tested in a particular facility, the only way to avoid diffuser breakdown is to improve the performance of the tested engine and to reduce the drag by the engine support rig.

VII. Conclusions

Drag, fuel supply, and thrust delivered by the tested engine were each represented by a point source to evaluate the effects on the diffuser flow in an engine wind tunnel. The following conclusions were obtained.

1) The total pressure of the test air was sufficiently high against the suction pressure of the exhaust system. On the other hand, the airflow tended to choke in the diffuser due to large drag and the heat release in engines in the test section.

2) The choking criterion in engine wind tunnels was analytically derived by one-dimensional flow analysis in conjunction with a chemical equilibrium code.

3) Inserting gas sampling probe rakes behind the engine nozzle caused greater drag in the diffuser flow. The drag lowered the Mach number in the diffuser flow and promoted thermal choking in engine tests.

4) Our RBCC engine may encounter diffuser breakdown because of the thrust and the drag performance. From our prediction of test cell pressure, the diffuser breakdown indicates that the propellant supply rate should be limited to 1.4 kg/s at most.

5) Momentum addition by an auxiliary ejector does not work for prevention of thermal choking. The efficiency of water spray to cool the total temperature of the airflow is also limited because the effect appears as the ratio between the heat of vaporization and the enthalpy of the air. At a given facility performance and engine size, the effective way to avoid thermal choking is to decrease the engine drag and/or increase the thrust performance.

References

[1] Chinzei, N., Mitani, T., and Yatsuyanagi, N., "Scramjet Engine Research in the National Aerospace Laboratory in Japan," *Scramjet Propulsion*, edited by Curran, E. T., and Murthy, S. N. B., AIAA, Reston, VA, 2000, pp. 159–222.

[2] Mitani, T., Sakuranaka, N., Tomioka, S., and Kobayasghi, K., "Boundary-Layer Control in Mach 4 and Mach 6 Scramjet Engines," *Journal of Propulsion and Power*, Vol. 21, No. 4, July–Aug., 2005, pp. 636–641.

[3] Mitani, T., Tomioka, S., Kanda, T., Chinzei, N., and Kouchi, T., "Scramjet Performance Achieved in Engine Tests from M6 to M8 Flight Condition," *12th AIAA Spaceplane and Hypersonic Systems and Technologies*, AIAA Paper 2003-7009, Dec. 2003.

[4] Ueda, S., Tomioka, S., Ono, F., Sakuranaka, N., Tani, K., and Murakami, A., "Mach 6 Test of a Scramjet Engine with Multi-Staged Fuel Injection," *44th AIAA Aerospace Sciences Meeting and Exhibit*, AIAA Paper 2006-1027, Jan. 2006.

[5] Mitani, T., Hiraiwa, T., Kanda, T., Shimura, T., Tomioka, S., Kobayashi, K., Izumikawa, M., Sakuranaka, N., Watanabe, S., Tarukawa, Y., Kouchi, T., Kitamura, E., and Yatsunami, T., "Subscale Wind Tunnels and Supplemental Studies of Scramjet Engine Tests," National Aerospace Lab., Tokyo, TR-1458, 2003, p. 227.

[6] Kanada, T., Tomiok, S., Ueda, S., Tani, K., and Wakamatsu, Y., "Design of Sub-Scale Rocket-Ramjet Combined Cycle Engine Model," *56th International Astronautical Congress*, International Astronautical Congress Paper IAC-05-C4.5.03, Oct. 2005.

[7] Sakuranaka, N., Mitani, T., Tomioka, S., Kato, K., Takegoshi, M., and Kudo, K., "Modifications of RJTF for Sea-Level Tests of a Combined Cycle Engine," *Proceedings of the Annual Meeting and the 6th Symposium on Propulsion System for Reusable Launch Vehicle*, Northern Section of Japan Society for Aeronautical and Space Sciences, Sendai, Japan, March 2006, pp. 177–182 (in Japanese).

[8] Shapiro, A. H., *The Dynamics and Thermodynamics of Compressible Fluid Flow*, Wiley, New York, Vol. 1, 1953, p. 219.

[9] Gordon, S., and McBride, B. J., "Computer Program for Calculation of Complex Chemical Equilibrium Compositions and Applications, I Analysis," NASA RP-1311, 1994.

[10] Rubesin, M. W., Mayden, R. C., and Varga, S. A., "An Analytical and Experimental Investigation of the Skin Friction of the Turbulent Boundary Layer on a Flat Plate at Supersonic Speeds," NACA TN2305, 1951.

[11] Kouchi, T., Mitani, T., and Masuya, G., "Numerical Experiments of Scramjet Combustion with Boundary-Layer Bleeding," *Journal of Propulsion and Power*, Vol. 21, No. 4, 2005, pp. 642–649.

[12] Tani, K., Kanda, T., Kato, K., Sakuranaka, N., and Watanabe, S., "Aerodynamic Performance of the Combined-Cycle Engine Inlet in a Supersonic Region," *Proceedings of 25th International Symposium on Space Technology and Science*, Japan Society for Aeronautical and Space Sciences and the Organized Committee of the 25th and the International Symposium on Space Technology and Science, Tokyo, June 2006, pp. 127–135.

R. Bowersox
Associate Editor